

Supporting Information

Charge-Transfer within Zr-Based Metal-Organic Framework: The Role of Polar Node

Andrea Van Wyk,^{a, †} Tanner Smith,^a Jaehong Park,^b and Pravas Deria^a*

^a Department of Chemistry and Biochemistry, Southern Illinois University, 1245 Lincoln Drive, Carbondale, Illinois 62901, United State.

^b Department of Molecular Engineering, Kyoto University, Katsura, Nishikyo-ku, Kyoto 615-8510, Japan

A. Materials

Solvents including acetone, *N,N*-dimethylformamide (DMF), were purchased from Macron. Spectroscopic grade solvents including 3-methyl pentane, toluene, 2-methyl tetrahydrofuran, α , α , α -trifluomethyl benzene (CF₃-Toluene), and acetonitrile were obtained from Sigma-Aldrich and were purged with nitrogen prior to spectroscopic study. Ferrocene carboxylic acid was obtained from Aldrich and was used as received. 1,3,6,8-tetrakis(*p*-benzoic acid)pyrene (H₄TBAPy) and activated microcrystalline NU-1000 were synthesized according to literature procedure.¹

B. Instrumentation

Powder X-ray diffraction (PXRD) patterns were recorded on a Rigaku Ultima IV diffractometer (measurements made over a range of $1.5^\circ < 2\theta < 30^\circ$ in a 0.05° step width with a 2 deg/min scanning speed).

Scanning Electron Microscopy (SEM) and Energy Dispersive Spectroscopic (EDS) data were collected at Image Center, SIU Carbondale. Elemental analysis was performed using a Quanta FEG 450 Scanning Electron Microscope (SEM) equipped with an Oxford INCA Energy Dispersive Spectroscopy (EDS) system. Dried samples were spread on double-stick carbon tape on an aluminum SEM sample holder and was used as is without coating to obtain better elemental data of Fe/Zr which was then converted to Fc/TBAPy (see **Figure S1**; **Table S1**).

Steady-State emission and excitation-emission mapping spectra were recorded at room temperature using Edinburg FS5 spectrofluorimeter. Samples for spectroscopic measurements were packed inside quartz capillary tube (ID = 3 mm), charged with nitrogen or respective solvent, and then sealed inside a glovebox. These capillary tubes were centrally-mounted on the solid sample module and spectra were collected in front-face configuration. Spectra were then collected using a 1.4 nm excitation and 0.4 nm emission slit width, and were corrected using the instrumental correction functions for the excitation light source as well as detector response. The absolute quantum yields were measured using a 150 mm integrating sphere. Solid crystalline powder loaded capillary tubes were centrally-positioned inside a 10×10 mm quartz sample holder. The reported values are the average of three separate measurements. Reference spectra for the QY measurement were collected using capillary tube filled with the corresponding dielectric medium. QY values were calculated F980 software.

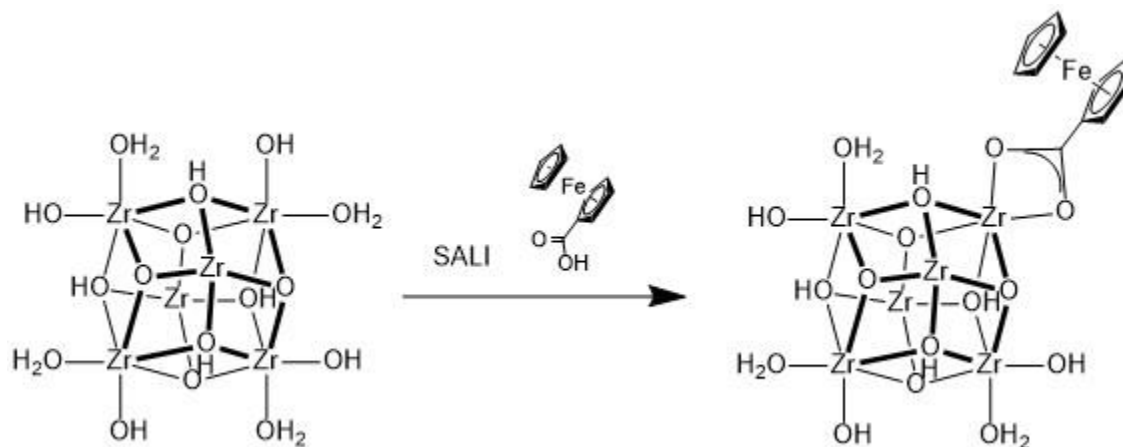
Fluorescence lifetime emission decay profiles and time-resolved emission spectra were recorded using an Edinburg Lifespec II Picosecond Time-Correlated Single Photon Counting spectrophotometer equipped with Hamamatsu H10720-01 detector and a 405 nm picosecond pulsed diode laser as TCSPC source. Instrumental control, kinetic data collection, processing and fitting were performed using F980 software. This instrument displays a measured instrumental response function of 180 ps; as such, reconvolution based exponential fitting using F980 software was used to extract lifetime data as low as 20 ps ($1/10^{\text{th}}$ the instrument response function).

Femtosecond pump/probe transient absorption spectroscopy experiments: Femtosecond transient absorption spectra were obtained using standard pump-probe methods (Ultrafast Systems, HELIOS, Sarasota, FL, United States). Optical pulses (<100 fs) centered at 800 nm are generated using a Ti:sapphire laser (Hurricane, Spectra-Physics, United States), which consists of a regenerative amplifier seeded by a mode-locked oscillator. The output of the regenerative amplifier is split to feed a Second Harmonic Generator (Spirit, Spectra-Physics, United States), which generates excitation pulses of 400 nm wavelength. The pump beam is chopped at half the

laser repetition rate (~ 500 Hz). The polarization and attenuation of the pump beam are controlled by half-wave plate and polarizer pairs. The pump beam polarization is set to the 54.7 degree with respect to the polarization of the probe beam for these experiments. The pump beam is focused into the samples with an $f = 200$ mm lens, while the probe beam is focused with a concave mirror. The spot size diameter of the pump beam is ~ 0.45 mm. The beam diameter is determined using Thorlab beam analyzer. The excitation pump pulse energy is measured using an energy meter (Ophir). A small fraction of the output from the regenerative amplifier is passed through an optical delay line and used to generate the white light continuum probe beam. This probe beam is split into two fractions before it passes through a sample, and one fraction is directed to a sample and a probe detector channel while the other fraction is directed to a reference detector channel. After passing through the sample, the probe light is adjusted using a variable neutral density filter and appropriate color glass filters to avoid saturating the detectors. Pairs of consecutive spectra are measured with $I_{\text{on}}(\lambda)$ and $I_{\text{off}}(\lambda)$ to determine the difference spectrum, $\Delta A = \log I_{\text{off}}(\lambda)/I_{\text{on}}(\lambda)$. All these experiments utilize a sealed quartz cuvette (2mm path length); all transient optical studies are carried out at 20 ± 1 °C. All transient spectra reported represent averages obtained over 5 scans, with each scan consisting of 500 frames with ~ 100 – 300 data points. Following all pump–probe transient absorption experiments, electronic absorption spectra verified that the samples were robust

C. Fc@NU-1000 sample preparation.

We implemented SALI to prepare **Fc@NU-1000** samples following a published procedure.² In brief, a 60 mg portion of activated pristine NU-1000 (0.023 mmol) was soaked in solutions containing various amounts of Fc-COOH (2 mM) solution in DMF in 10 mL vials, which was then capped and heated at 60 °C for 24 h with occasional swirling. The supernatant of the reaction mixture was decanted and the MOF sample was soaked, centrifuged and washed with fresh DMF five times over the course of 2 days. The solid was soaked (overnight) and washed with acetone (4×15 mL), and finally dried in a vacuum desiccator (~100 torr). The loadings of Fc-COO⁻ at the node were determined via SEM-EDS elemental analysis and corroborated with ICP-MS data.



Scheme S1. Installation of **Fc-COO⁻** in NU-1000 via SALI.

Table S1. Fc/TBAPy ratio obtained from SEM-EDS data

Sample	Intended Fc/TBAPy ratio loaded in SALI	Fc/TBAPy ratio from SEM-EDS
F	0.0067	0.006
E	0.016	0.015
D	0.029	0.030
C	0.100	0.093
B	0.250	0.175
A	0.500	0.353

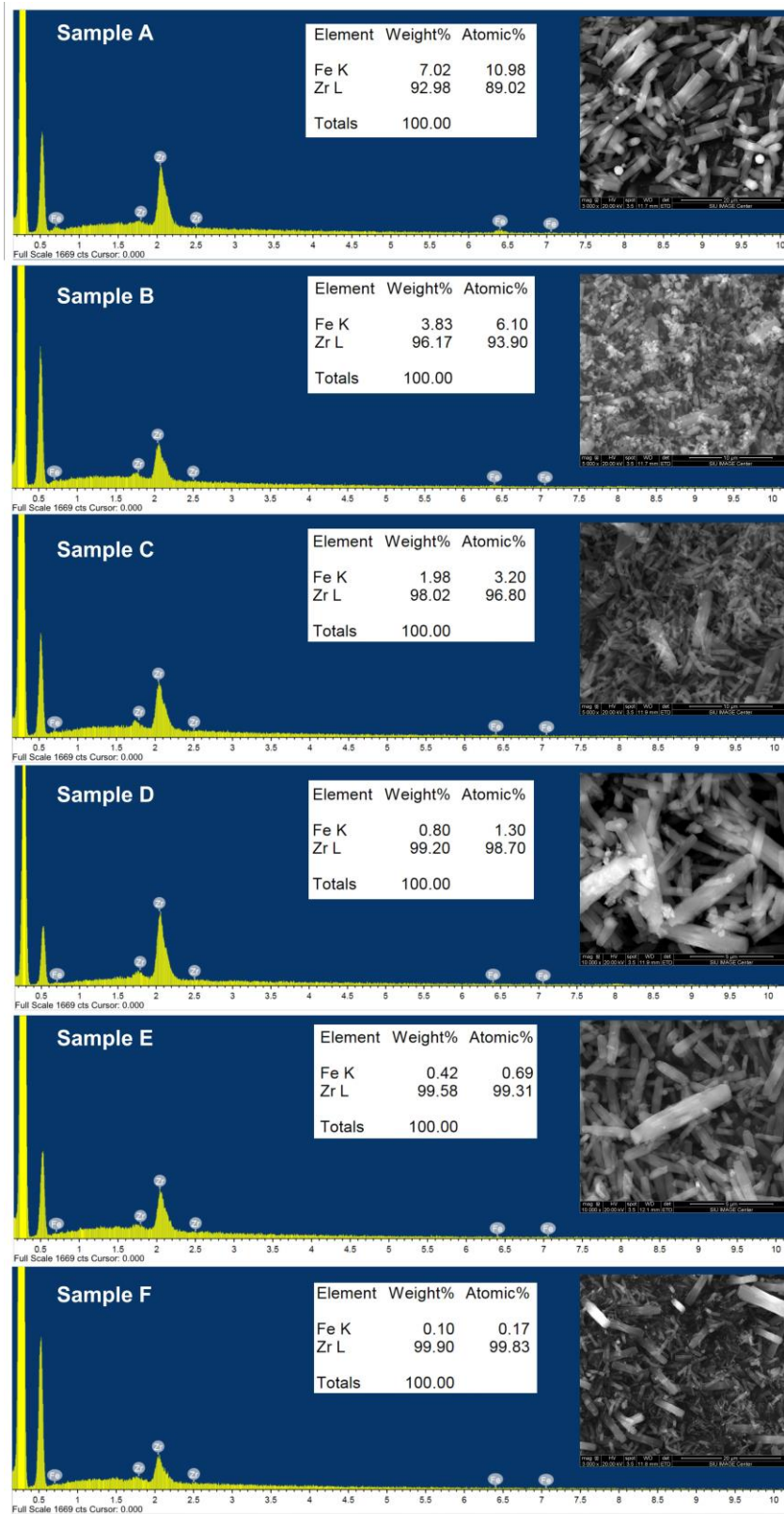


Fig. S1. SEM pictures and the EDS spectra of the Fe-COO doped NU-1000 samples (inset showing Fe/Zr atom ratio).

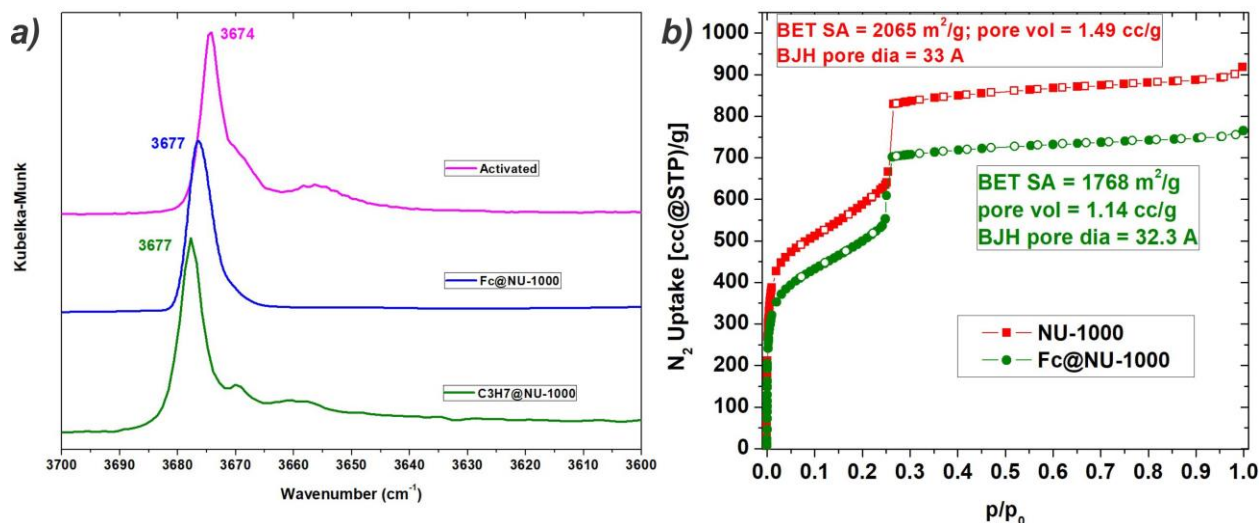


Figure S2. (a) DRIFTS plots of the **FC@NU-1000** (sample A; blue) highlighting the stretching frequency of the bridging and remaining terminal hydroxyl and aqua ligands upon Fc-attachment relative to the unmodified NU-1000 (pink) sample. For comparison, DRIFTS of a butanoate modified NU-1000 sample (green). (b) N_2 isotherms (at 77K) of **FC@NU-1000** (green) and NU-1000 (red) highlighting reduction of surface area, pore volume and pore diameter upon Fc functionalization.

To perform fs-TA and relevant spectroscopic experiments, microcrystalline samples were necessary (for the probe light to transmit through a suspension following the excitation by the pump beam). Chosen micron sized crystals are not suitable for single crystal X-ray data collection. To check if the Fc-COO^- are indeed bound to the $\text{Zr}^{\text{IV}}\text{-oxo}$ node pointing to the mesopores of NU-1000, we collected DRIFTS data and N_2 isotherm. SALI (**Figure 1d**; **Scheme S1**) functionalization involves an established chemistry² that allows attachment of an incoming carboxylate based ligand (i.e. Fc-COO^-) to the open sites of an 8-connected $\text{Zr}^{\text{IV}}\text{-oxo}$ node by replacing a pair of terminal hydroxyl and aqua ligands. Thus, **FC@NU-1000** samples, previously reported compositions,³ show unique hydroxyl stretching (**Figure S2**) at 3677 cm^{-1} similar to a SALI derived $\text{C}_3\text{H}_7\text{-COO}^-$ bound NU-1000. This stretching frequency is clearly distinct from the original 3674 cm^{-1} peak seen for unmodified sample and matches to the literature reports.² Furthermore, the N_2 -isotherm data collected for **FC@NU-1000** sample at 77 K highlights a reduction in BET surface area and pore volume compared to an unmodified NU-1000 sample. The N_2 -isotherm data presented in **Figure S2** also indicates a reduction of pore diameter by $\sim 1\text{ \AA}$. Note that the sample used to collect the N_2 isotherm contains only ~ 0.7 Fc-COO^- moiety per node, where a maximum of four Fc-COO^- ligands can be loaded; this small reduction in pore diameter only validates that the Fc moiety is indeed positioned at very close proximity to the node. With these experimental data indicating a node bound Fc-COO^- system, we utilized DFT modelling to find its position relative to the TBAPy linkers. Since the Fc-COO^- moiety is directly attached to the node through a carboxylate functionality without any flexible tether, the DFT computation highlights a ‘fixed’ positioning of the pendant Fc-COO^- enforced by the adjacent phenyl rings of the TBAPy linkers and a strain stemming from dihedral angle between the carboxy group and the cyclopentenyl group.

Computational Methods. Structure of the Fc-COO^- bound node relative to the TBAPy linkers was studied with a truncated model shown in **Figure 1** in the main text using density functional theory (CAM-B3LYP/LANL2DZ; Gaussian-09 software⁴ package). Structures of the model compound were constructed from the crystallographic coordinates of one $\text{Zr}^{\text{IV}}\text{-oxo}$ node that holds one Fc-COO^- and four adjacent TBAPy linkers. To perform an affordable computation, eight of the neighboring $\text{Zr}^{\text{IV}}\text{-oxo}$ nodes were removed and a proton was introduced to the carboxylates groups for charge balance. A constrained DFT optimization was performed by keeping all the framework atoms fixed to their crystallographic coordinates and only the atom of node bound “ Fc-COO^- ” moiety were allowed to move.⁵

D. Spectroscopic data.

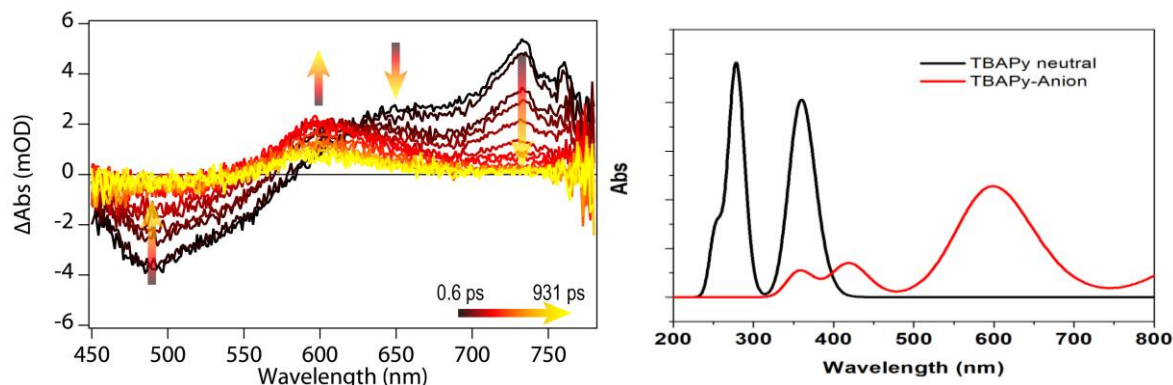


Figure S3. (Left) Femtosecond transient absorption spectra of **Fc@NU-1000** in toluene solvent. Experimental condition: $\lambda_{\text{ex}} = 400$ nm; Fc/TBAPy = 0.175. (right) TDDFT (CAM-B3LYP/LANL2DZ;⁶ Gaussian-09 software⁴ package) computed absorption spectra of TBAPy (black) and TBAPy⁻ species showing 600 nm transition for the later.

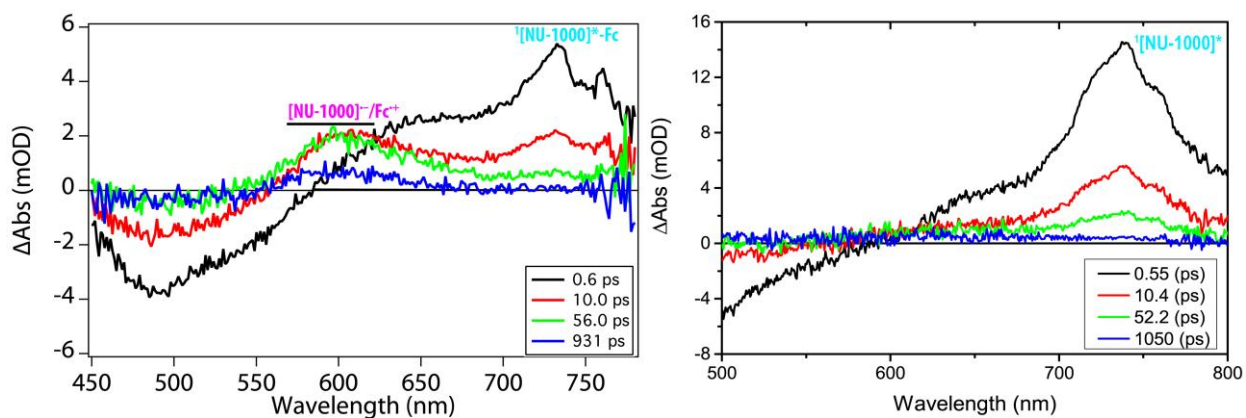


Figure S4. Femtosecond transient absorption spectra of (left) **Fc@NU-1000** in toluene solvent and (right) pristine NU-1000 in polystyrene matrix shown at comparable delay times. Experimental condition: $\lambda_{\text{ex}} = 400$ nm; Fc/TBAPy = 0.175.

Table S2: Absolute emission quantum yields of **Fc@NU-1000** samples with varying degree of Fc/TBAPy ratio measured at ambient temp in different solvents.

QY Sample media	U	F	E	D	C	B	A
Air	5.35	2.48	2.17	1.24	0.61	0.1	0.088
MePent	19.5	9.6	7.8	3.24	1.61	0.49	0.199
Tol	17.3	10.9	8.96	4.13	1.38	0.433	0.202
MeTHF	20.8	10.8	9.75	4.46	1.36	0.48	0.252
CF3Tol	13.0	8.56	7.09	3.17	1.41	0.38	0.211
MeCN	6.2	6.58	5.61	2.36	1.53	0.503	0.18

Sample Identity: 0.000 (U), 0.006 (F), 0.015 (E), 0.030 (D), 0.093 (C), 0.175 (B), and 0.353 (A)

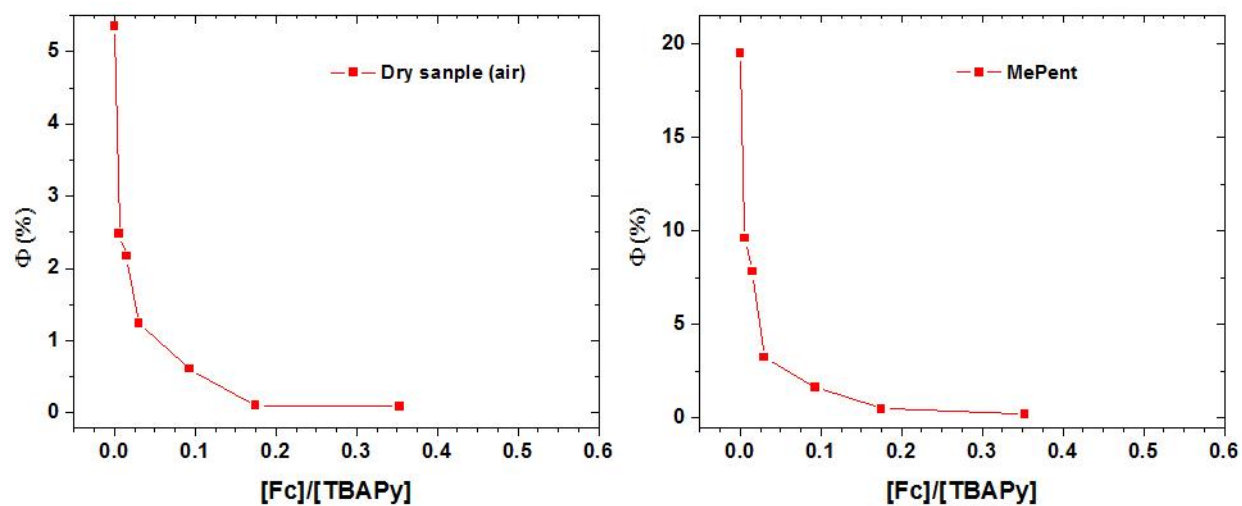


Figure S5. Steady-state emissive data showing a monotonous quenching of absolute quantum yield with the increase in the ferrocene loading.

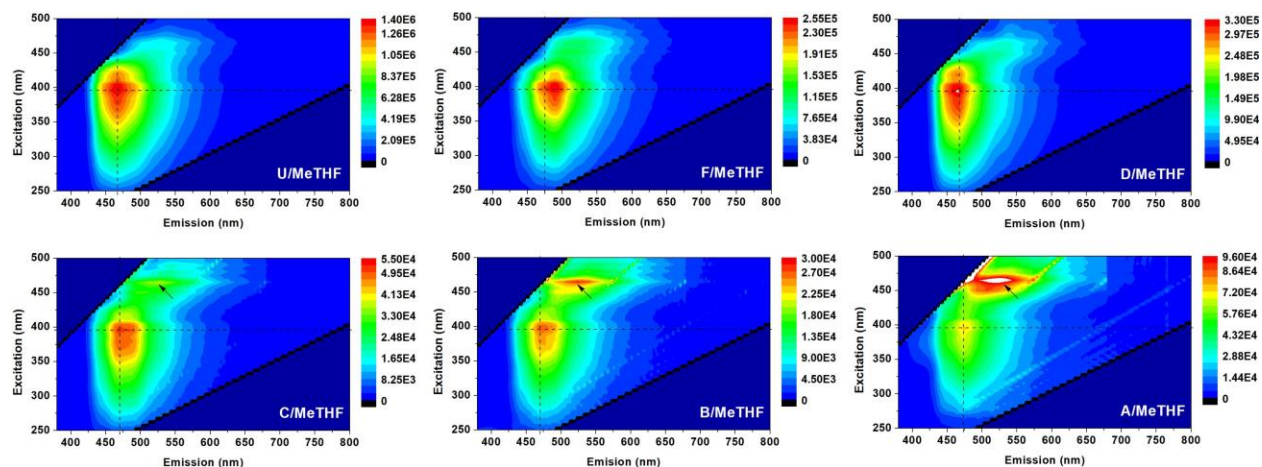


Figure S6. Excitation-emission mapping of **Fc@NU-1000**. The arrows in samples C-A denote residual low energy emission from a small amount of NU-901 impurity. Experimental condition: solvent = 2-methyl tetrahydrofuran; $T = 298$ K; the Fc:TBAPy ratio: 0.000 (U), 0.006 (F), 0.015 (E), 0.030 (D), 0.093 (C), 0.175 (B), and 0.353 (A).

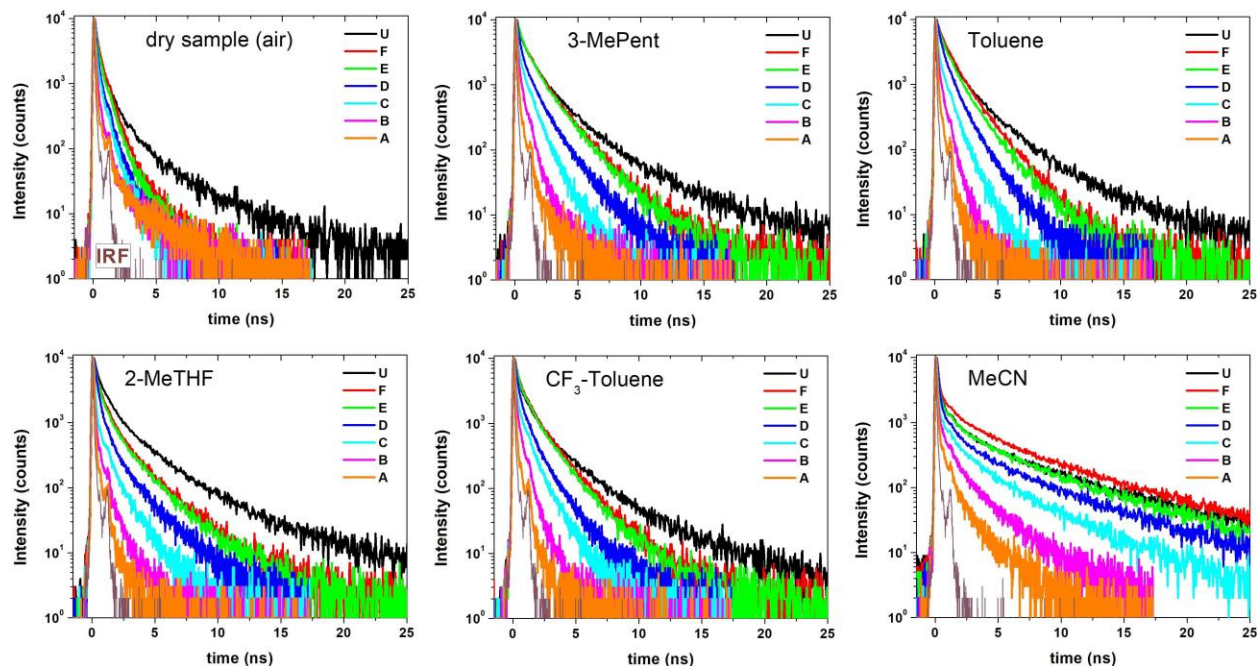


Figure S7. Transient emission decay profiles of **Fc@NU-1000** with varying Fc/TBAPy ratio and dielectric highlighting fast decay with increase in Fc/TBAPy ratio. [Data collected at the emission $\lambda_{\max} = 470$ nm and $\lambda_{\text{ex}} = 405$ nm]. Note, a long lived component significantly contributes in the MeCN solvent thus make the kinetic data summarized in Table 1 (main text) slower.

Table SI-3. Emission Lifetime (ns; major fast component) Data for **Fc@NU-1000** Samples with varying Fc/TBAPy ratio and dielectric.

media	U (%)	F (%)	E (%)	D (%)	C (%)	B (%)	A (%)
Air	0.62 (82)	0.48 (88)	0.43 (87)	0.30 (86)	0.32 (90)	0.21 (90)	0.20 (93)
MePent	1.12 (73)	0.78 (60)	0.75 (60)	0.54 (67)	0.37 (70)	0.27 (88)	0.18 (95)
Tol	1.13 (74)	0.70 (52)	0.71 (62)	0.51 (68)	0.41 (71)	0.22 (80)	0.23 (97)
MeTHF	1.10 (70)	0.65 (68)	0.51 (65)	0.38 (72)	0.37 (80)	0.23 (88)	0.35 (98)
CF3Tol	0.90 (68)	0.64 (54)	0.64 (58)	0.41 (70)	0.41 (73)	0.25 (86)	0.11 (90)
MeCN	1.26 (50)	1.31 (45)	1.16 (50)	0.99 (58)	0.98 (63)	0.53 (73)	0.52 (98)

Sample Identity: FC/TBAPy: 0.000 (U), 0.006 (F), 0.015 (E), 0.030 (D), 0.093 (C), 0.175 (B), and 0.353 (A). Data collected at the emission $\lambda_{\max} = 470$ nm and $\lambda_{\text{ex}} = 405$ nm. Note, a long lived component significantly contribute in the MeCN solvent thus make the kinetic data summarized in Table 1 (main text) slower.

E. References

1. Wang, T. C.; Vermeulen, N. A.; Kim, I. S.; Martinson, A. B. F.; Stoddart, J. F.; Hupp, J. T.; Farha, O. K. *Nature Protocols* **2016**, *11*, 149.
2. (a) Deria, P.; Mondloch, J. E.; Tyljanakis, E.; Ghosh, P.; Bury, W.; Snurr, R. Q.; Hupp, J. T.; Farha, O. K. *J. Am. Chem. Soc.* **2013**, *135*, 16801; (b) Deria, P.; Bury, W.; Hod, I.; Kung, C.-W.; Karagiari, O.; Hupp, J. T.; Farha, O. K. *Inorg. Chem.* **2015**, *54*, 2185; (c) Deria, P.; Bury, W.; Hupp, J. T.; Farha, O. K. *Chem. Commun.* **2014**, *50*, 1965; (d) Deria, P.; Chung, Y. G.; Snurr, R. Q.; Hupp, J. T.; Farha, O. K. *Chem. Sci.* **2015**, *6*, 5172.
3. (a) Hod, I.; Bury, W.; Gardner, D. M.; Deria, P.; Roznyatovskiy, V.; Wasielewski, M. R.; Farha, O. K.; Hupp, J. T. *J. Phys. Chem. Lett.* **2015**, *6*, 586; (b) Hod, I.; Farha, O. K.; Hupp, J. T. *Chem. Commun.* **2016**, *52*, 1705.
4. Frisch, M. J.; Trucks, G. W.; Schlegel, H. B.; Scuseria, G. E.; Robb, M. A.; Cheeseman, J. R.; Scalmani, G.; Barone, V.; Mennucci, B.; Petersson, G. A.; Nakatsuji, H.; Caricato, M.; Li, X.; Hratchian, H. P.; Izmaylov, A. F.; Bloino, J.; Zheng, G.; Sonnenberg, J. L.; Hada, M.; Ehara, M.; Toyota, K.; Fukuda, R.; Hasegawa, J.; Ishida, M.; Nakajima, T.; Honda, Y.; Kitao, O.; Nakai, H.; Vreven, T.; Montgomery, J. A., Jr.; Peralta, J. E.; Ogliaro, F.; Bearpark, M.; Heyd, J. J.; Brothers, E.; Kudin, K. N.; Staroverov, V. N.; Kobayashi, R.; Normand, J.; Raghavachari, K.; Rendell, A.; Burant, J. C.; Iyengar, S. S.; Tomasi, J.; Cossi, M.; Rega, N.; Millam, J. M.; Klene, M.; Knox, J. E.; Cross, J. B.; Bakken, V.; Adamo, C.; Jaramillo, J.; Gomperts, R.; Stratmann, R. E.; Yazyev, O.; Austin, A. J.; Cammi, R.; Pomelli, C.; Ochterski, J. W.; Martin, R. L.; Morokuma, K.; Zakrzewski, V. G.; Voth, G. A.; Salvador, P.; Dannenberg, J. J.; Dapprich, S.; Daniels, A. D.; Farkas, Ö.; Foresman, J. B.; Ortiz, J. V.; Cioslowski, J.; Fox, D. J. *Gaussian 09*, Revision D.01; Gaussian Inc.: Wallingford CT, 2009.
5. (a) Deria, P.; Gómez-Gualdrón, D. A.; Hod, I.; Snurr, R. Q.; Hupp, J. T.; Farha, O. K. *J. Am. Chem. Soc.* **2016**, *138*, 14449; (b) Deria, P.; Yu, J.; Balaraman, R. P.; Mashni, J.; White, S. N. *Chem. Commun.* **2016**, *52*, 13031.

6. (a) Yanai, T.; Tew, D. P.; Handy, N. C. *Chem. Phys. Lett.* **2004**, 393, 51; (b) Dunning Jr., T. H.; Hay, P. J., *Modern Theoretical Chemistry*. Plenum, New York, 1977; Vol. 3.